Hierarchical interconnections in the nano-composite material Bone: Fibrillar Cross-Links resist fracture on several length scales

Georg E. Fantner[1,*], Olexandr Rabinovych[2], Georg Schitter[1], Philipp Thurner[1], Johannes H. Kindt[1], Marquesa M. Finch[1], James C. Weaver[3], Laura S. Golde[1], Daniel E. Morse[3], Everett A Lipman[1], Ivo W. Rangelow[2], Paul K Hansma[1]

[1] University of California Santa Barbara, Department of Physics, CA 93106 Santa Barbara, USA

[2] University of Kassel, Institute for Microstructuretechnologies and Analytics, Heinrich-Plett-Str. 40, 34132 Kassel, Germany

[3] University of California Santa Barbara, Institute for Collaborative Biotechnologies, CA 93106 Santa Barbara, USA

[*] corresponding author: fantner@physics.ucsb.edu

Abstract:

Bone is a complex and very important multi-constituent bio-composite. In this work, we focus on the arrangement of bone constituents from the nanoscopic to the microscopic scale, and investigate the influence of their arrangements on the fracture mechanisms of the whole composite. We find that bone, on the nanoscopic scale, consists of mineralized collagen fibrils held together by a non-fibrillar organic matrix, which results in a primary failure mode of delamination between mineralized fibrils. In turn, these mineralized fibrils form one of three types of filaments that span microcracks in fractured bone samples, possibly resisting the propagation of these cracks.

Bone is one of the most important and most complex biominerals. It has become the focus of intensive study in light of the rising average population age and associated bone diseases. In recent years, it has become increasingly clear that, in addition to the insights achieved in the biological sciences and medicine, information on the nanoscopic architecture of the bone is needed to understand and predict bone fracture, e.g. [1]. Bone consists mainly of mineralized collagen fibrils. The collagen fibrils, being the main organic component in bone, are reinforced with nanoscale hydroxyapatite particles [2-8]. This results in a mineral reinforced protein fibril of approximately 50-100 nm diameter. These fibrils are the elementary building block for the large variety of bones in the body. To facilitate the function of the specific bone, they are arranged in several possible patterns [9].

In addition to its biomedical significance, bone has been used as a model for many artificial bio-ceramic composites [10, 11]. In many of these artificial composites, a combination of a soft polymer matrix reinforced with stiff particles is used as an approximation of the interaction between collagen and hydroxyapatite. Such materials are based on the crystal-polymer interactions on the molecular and nanoscopic level. In this paper, we present additional strength-increasing mechanisms in bone that may add to the quality of artificial bio-mineral composites.

Materials and Methods:

Trabecular bone samples were cut from fresh bovine and human vertebrae. Samples were frozen and cut on a band saw into cubes approximately 4.5x4.8x4.0 mm, where the shortest dimension was in the direction of the spinal column. The marrow was removed from the trabeculi using a pressurized stream of phosphate buffered saline (PBS) solution or water.

A buffer (40 mM CaCl, 110 mM NaCl, 10 mM HEPES, brought to pH 7.0 by addition of small amounts of 1.0 M NaOH) was used for storage.

Atomic Force Microscopy (AFM):

Single trabeculae were extracted from human and bovine bone cubes under a dissecting microscope and mounted on steel sample discs with 2-ton epoxy. The samples were then rinsed in de-ionized water. Remaining water was removed by placing the mounted samples in a centrifuge tube on top of a Kimwipe. The samples were centrifuged for a few seconds after which all samples were placed in a vacuum desiccator and evacuated to

below 1 Torr. Samples were imaged in contact mode (Figure 1A) or tapping mode (Figure 1B) under nitrogen atmosphere.

Scanning Electron microscopy (SEM): Trabecular bone cubes were polished and cleaned with pressurized water to remove loose residues. The bone samples were compressed (under PBS solution) in a small, SEM-compatible vise that fits in the chamber of an FEI (XL 40 Sirion) Scanning Electron Microscope. After compression, residual salts were removed by immersing the clamped sample in a Milli-Q (Millipore-purified) water-supplied flow-through system. The samples were then dried in a vacuum oven (10^{-3} Torr, 30^{o}C) and gold/palladium-coated by sputtering for SEM imaging.

Human trabecular bone was purchased from a tissue bank and prepared using the same procedure as used for the bovine the bovine bone. All the images chosen for this paper are representative examples of features observed several times in different samples of human as well as bovine bone.

Environmental SEM:

Bone samples were extracted from bovine vertebrae in the same way as for the conventional SEM images. Samples were then cut into 1mm thick slices and sanded with 1200 grit sandpaper. The sample was placed in a custom made holder in which it could be loaded while mounted on the stage of an Environmental Scanning Electron Microscope (ESEM, Philips XL30). The samples were kept in storage buffer and the uncoated samples were loaded in the ESEM while being moist. In the ESEM, excess water was evaporated through the vacuum system. The sample was cooled to 3°C in an

environment of close to 100% humidity. The preloaded sample was imaged to find a suitable crack with bridging fibrils. To further strain the bone, the chamber of the ESEM was vented and the sample was rewetted. The strain was increased by tightening a clamping screw in the custom sample holder. After blotting the sides of the sample with a Kimwipe and evaporation of the excess water in the vacuum chamber of the ESEM, the crack was relocated and imaged.

Nanojet:

Nanojet (Nanonozzle Plasma JET Microfabrication Tool) is a new tool for nanoscale localized chemical etching by gaseous species (free radicals)[12, 13]. Radicals are created from a mixture of two gases (SF_6 and O_2) within a cavity, powered by a microwave generator, operating at 100 W and 2.45 GHz (Electro-Medical Supplies). The radicals are transported through a capillary, which is tapered to form a nanonozzle. The electrically neutral radicals are forced in the direction of the substrate by a pressure gradient along the tube. In contrast to kinetic etch techniques such as Focus Ion Beam (FIB) which operate with high-energy ions (5-100 keV), the chemically active radicals in Nanojet have thermal energy and therefore do not mechanically damage the bone surface. Chemical etching of the substrate takes place at the surface only, leading to high selectivity of the etching with respect to different materials or their densities in the composite.

Due to the directionality of the molecular beam emerging from the high aspect ratio nanonozzle, a localized etching can be performed. By scanning the substrate under the nozzle, a pattern can be generated with nearly the same resolution as the nozzle diameter.

We etched the sample for one hour with a nozzle opening of 300 nm, which was positioned 100 nm above the sample. The sample was imaged by SEM after the first etch to observe the changes on the bone surface. To find the same place on the bone surface after each treatment and to see the evolution of the surface morphology, the surface was mechanically marked, which made it easily detectable during the SEM imaging. The formed topological details were also used to navigate and find the same surface area.

The etch procedure was repeated three times, where after each etch, the same spot was imaged. For SEM imaging we used a cold field emission electron microscope from Hitachi, Type 4000. To achieve high resolution images without the need for a metal coating, the sample was covered with metal mash grid, in order to avoid excessive charging of the sample while imaging.

Results:

Figure 1A shows an Atomic Force Microscopy image of collagen fibrils on the outside of human bone, showing the characteristic 67 nm banding periodicity on the surface of the fibril [14-16]. These fibrils are similar to fibrils observed on the outside of bovine bone [17]. Figure 1B shows an AFM image of a fractured surface of bovine bone at the same magnification as Figure 1A, showing collagen fibrils coated with hydroxyapatite particles [5, 17, 18]. These mineralized collagen fibrils form the basic building block of bone. In bone, they are held together by a non-fibrillar organic matrix as can be seen in Figure 2. The amount of this non-fibrillar organic matrix and the degree of mineralization can vary strongly between bone samples and even within the same sample [19-22]. Figure 2 shows

SEM images of osteoporotic human trabecular bone from spots within a 2×2 mm area and reveals great variations in the amount of non-fibrillar organic matrix. Figure 2A shows mineralized collagen fibrils that are interconnected with a large amount of unmineralized, non-fibrillar organic matrix. The fibrils are completely coated but the mineral particles can be seen slightly through the smooth layer. Figure 2B shows an area on the same sample with a large amount of unmineralized collagen fibrils showing the characteristic 67 nm banding pattern. Between the collagen fibrils, particles can be seen, but the fibrils are not as fully mineralized as the fibrils in Figure 1B. Figure 2C shows an area where little to no non-fibrillar organic matrix interconnects the mineralized fibrils. The fibrils are packed loosely, with many voids between the fibrils compared to the fibrils in Figure 2A. Figure 2D shows a crack formation in an area with a large amount of non-fibrillar organic matrix. The organic matrix forms filaments that span the small microcrack, putatively resisting the growth and propagation of the microcrack.

To investigate whether there are mineralized collagen fibrils underneath the non-fibrillar matrix in Figure 2, and whether this non-fibrillar matrix is indeed organic, we used a novel nanostructuring tool (Nanojet) to selectively remove the organic layer [12]. Nanojet uses a localized beam of thermal reactive radicals to selectively remove organic components: Figure 3A shows the schematic principle of this instrument. Using the beam of reactive radicals, a fracture surface of cortical bone was etched for one hour and then imaged by SEM. This procedure was repeated a total of three times, where after each etch, the same spot was imaged. The resulting SEM images after one, two, and three hours of etching are shown in Figure 3B, C, and D respectively. In Figure 3B, the superficial

organic layer has been removed by Nanojet and the crystals underneath can be seen. As more organic material is removed, more of the fibrillar structure is revealed (Figure 3C). After three hours of etching, the organic material has been removed deep into the bone. The structures in Figure 3D remain fibrous even though most of the organic material has been removed.

The fibrous architecture of bone has profound influence on the formation and orientation of microcracks in bone [23], which are believed to be an important precursor for bone failure [21, 24, 25]. Figure 4A shows the tip of a delamination crack in bovine trabecular bone. The crack forms along the direction of the mineralized fibrils which are parallel to the surface of the trabeculi. Within the crack, the fracture surface has a fibrous appearance and filaments can be seen to span the extent of the crack (Figure 4B). Such filaments have been reported in human cortical bone [26] and it has been suggested that they contribute to the fracture toughness of bone [27]. Most of these filaments originate from previously parallel-laying fibrils. When a crack is formed, the parallel mineralized collagen fibrils must be separated (Figure 4C). The binding between the mineralized fibrils leads some fibrils to be connected to both sides of the crack and thereby to form filaments between the two crack surfaces which might resist the further growth of the crack. These mineralized collagen fibrils are the main filament type that span microcracks, representing approximately 95% of all the cross-linking filaments we observed (Figure 4E, filament 1). Another type of filament is unstructured, forming stringy cross-links as seen in Figure 4E, filament 2. This type of filament may consist of the same non-fibrillar organic matrix that holds the mineralized collagen fibrils together

(Figure 2A, B). The third type of filament is represented by unmineralized collagen fibrils, Figure 4E, filament 3. These fibrils show the characteristic 67nm banding pattern of collagen (see white arrows in Figure 4F). In addition to this typical banding pattern, a second smaller banding pattern can be seen. This banding pattern has a periodicity of ≈ 22 nm and is similar to a small banding pattern in collagen recently found by AFM [15].

To open an existing crack, the cross-linking filaments must be overcome. This could be accomplished through 1) delamination of the fibrils from one surface (as suggested by Figure 4D) or 2) rupture of the fibrils. Figure 5A shows a crack in bovine trabecular bone with mineralized fibrils spanning the gap, in an image taken with environmental SEM. Figure 5B shows a higher magnification of a bundle of fibrils that span the crack. After additional load is applied on the sample, the crack opens, and the fibril bundle breaks (Figure 5C).

On the microscopic scale, mineralized collagen fibrils can have several arrangements, depending on the type and the specific function of the bone they form [28, 29]. In trabecular bone the fibrils are arranged to form a bi-continuous network of trabeculae and voids which are filled by bone marrow (see Figure 6). This type of bone is found mainly in vertebrae and long bones. Figure 7 shows a bovine trabecular bone sample fractured in tension parallel to the main fibrillar plane. The mineralized fibrils that form the trabeculae are generally oriented along the shape of the trabeculae (Figure 7A), which results in an anisotropy of the mechanical properties of the trabeculae and the trabecular bone as a whole [30-33]. On the fracture surface of Figure 7B, the fibrils have

delaminated in bundles, which consist of several mineralized collagen fibrils. The majority of the fibrils in the bundles are parallel to each other; however some fibrils are orthogonal to the bundles and interconnect the bundles (Figure 7C). The orthogonal bundles appear to also consist of mineralized fibrils and could act as resisting elements against the delamination (Figure 7D).

Discussion:

The fibrillar multi-component structure of bone results in cross-links on several size scales which consist of different materials. The cross-links on the nano scale between the mineralized fibrils consist predominately of non mineralized organic material, whereas the cross links between the microcracks and bundles of fibrils consists predominately of mineralized collagen fibrils. Whether and how these cross links contribute to the mechanical properties of bone remains unclear. It has been proposed that collagen fibrils that span between crack surfaces could increase the fracture toughness of bone [27]. In that work, Yeni and Fyhrie hypothesize that collagen fibrils that span microcracks exert a *crack closure stress* which resists opening of the crack and thereby reduces the probability that a crack will grow. Recently, Nalla et al. reported *uncracked ligament bridges* in cortical human bone [26] where they show some evidence that these filaments act as a toughening mechanism in bone. The three types of filament bridges in Figure 4E are all possible candidates for such a toughening mechanism. Since the majority of the bridging filaments are mineralized collagen, these fibrils will likely have the largest

contribution to this mechanism. In this case, the bonding between the mineralized fibrils is a determining factor of the effectiveness of the bridging mechanism [27].

There are several possible mechanisms by which the mineralized collagen fibrils that span cracks could be held to the sides of the microcrack. As can be seen in Figure 4D, the mineralized fibrils can be entangled with the fibrils of the bulk material. The rough texture of the fibril could increase the strength of the entanglement through interfibrillar friction. Alternatively or in combination with this, the material that is between the mineralized collagen fibrils in Figure 2 could also be partially responsible for keeping the mineralized fibrils attached to both sides of an opening microcrack (see Figure 4). As shown in Figures 2A and D, the bonding between the mineralized fibrils seems to be achieved by an unmineralized non-fibrillar organic matrix. The filaments that span the crack in Figure 2D suggest that the non-fibrillar organic matrix resists the opening of the crack. This non-fibrillar organic matrix would thereby act as a glue to hold the mineralized fibrils together. The composition of this "glue" is unclear. We hypothesize that it consists of any of the various bone associated polymers such as proteoglycans [34-37], non-fibrillar collagen [34] or bone sialoprotein [38].

The function of the organic matrix as a glue is supported by findings of Thompson et al. [39], who report that sacrificial bonds are present within the bone matrix. Such sacrificial bonds have also been shown for other bio-mineral systems such as abalone nacre, where the organic material glues aragonite plates together [40], contributing to the measured >1,000-fold increase in fracture toughness of the composite relative to the mineral alone.

These sacrificial bonds are weak, reformable bonds that increase the energy required to stretch molecules and thereby increase the energy that is required to break the molecules. When strain on the material is removed, these sacrificial bonds can reform; they therefore provide a mechanism for repeatable energy dissipation.

We hypothesize that the glue between the mineralized fibrils in Figure 2 serves a similar purpose. In order for the mineralized fibrils to separate, these glue bonds between the mineralized fibrils have to be broken. This mechanism could be reversible if the glue bonds reform when the microcrack relaxes, as suggested by Thompson et al. for the sacrificial bonds in bone [39]. The effectiveness of the mineralized fibrils that span the cracks to prevent crack propagation would in that case strongly depend on the condition of the non-fibrillar organic matrix. Degradation of this matrix would result in a decreased fracture toughness of the whole composite. Genetic knock-out studies in rats have shown that if the animal can no longer produce biglycans, a possible constituent of the organic matrix, the bone becomes weaker [41]. However, the inability to produce biglycans also affects many other parameters that contribute to bone fracture, so the connection between biglycans and the organic matrix is speculative.

We conclude that bone has a large variety of cross-links on various size scales. These cross-links could significantly contribute to the fracture toughness of bone. We hypothesize that mineralized fibrils are bonded together with a non-fibrillar organic matrix which might act as glue. These mineralized fibrils in turn span microcracks and crack tips, where they presumably resist the propagation of the cracks. The details of this

mechanism still have to be investigated. Future investigations into the composition of the non-fibrillar organic matrix will be necessary to better understand bone failure from the molecular to the macroscopic scale. The results of this paper suggest that there are multiple orders of complexity and strategies used to give bone its remarkable properties, which, when understood, may be useful to make higher performance artificial nano-composite materials.

Acknowledgements:

The Authors would like to thank Herbert Waite, Simcha Frieda Udwin, and Patricia Turner for their suggestions and fruitful discussions. We thank Gelson's Markets, Santa Barbara, especially Phil Vega for supplying fresh bovine vertebrae. José Saleta for assistance with ESEM experiments and Jan Lövander for assistance with high resolution SEM images.

Research supported by: NASA University Research, Engineering and Technology Institute on Bio Inspired Materials under award No. NCC-1-02037, NIH under award number GM65354, NSF under award number DMR-9988640, the Institute for Collaborative Biotechnologies through grant DAAD19-03-D-0004 from the U.S. Army Research Office, Veeco Instruments, the UCSB Materials Research Laboratory under NSF award DMR00-80034, the NOAA National Sea Grant College Program, U.S. Dept. of Commerce (NA36RG0537, Project R/MP-92) through the California Sea Grant College System. This work made use of MRL Central Facilities supported by the MRSEC Program of the National Science Foundation under award No. DMR00-80034.

ESEM imaging was done at MEIAF (Micro Environmental Imaging and Analysis Facility), Donald Bren School of Environmental Science and Management, funded by NSF 9977772.

GF thanks the Austrian Academy of Science for a DOC scholarship. GS thanks the Austrian Science Fund for support under project number J2395-N02. PT thanks the Swiss National Fund. MF thanks the UCSB RISE program. LG thanks the UC LEADS and UCSB RISE programs.

References:

1. Fratzl, P., et al., *Structure and mechanical quality of the collagen-mineral nano-composite in bone.* Journal of Materials Chemistry, 2004. **14**(14): p. 2115-2123.
2. Rosen, V.B., L.W. Hobbs, and M. Spector, *The ultrastructure of anorganic bovine bone and selected synthetic hyroxyapatites used as bone graft substitute materials.* Biomaterials, 2002. **23**(3): p. 921-928.
3. Tong, W., et al., *Size and shape of mineralites in young bovine bone measured by atomic force microscopy.* Calcified Tissue International, 2003. **72**(5): p. 592-598.
4. Eppell, S.J., et al., *Shape and size of isolated bone mineralites measured using atomic force microscopy.* Journal of Orthopaedic Research, 2001. **19**(6): p. 1027-1034.
5. Erts, D., L.J. Gathercole, and E.D.T. Atkins, *Scanning Probe Microscopy of Intrafibrillar Crystallites in Calcified Collagen.* Journal of Materials Science-Materials in Medicine, 1994. **5**(4): p. 200-206.
6. Follet, H., et al., *The degree of mineralization is a determinant of bone strength: a study on human calcanei.* Bone, 2004. **34**(5): p. 783-789.
7. Ziv, V. and S. Weiner, *Bone Crystal Sizes - a Comparison of Transmission Electron-Microscopic and X-Ray-Diffraction Line-Width Broadening Techniques.* Connective Tissue Research, 1994. **30**(3): p. 165-175.
8. Carlstrom, D., *Particle Size and Chemical Composition of the Crystallites in Bone and Synthetic Apatites.* Biochimica Et Biophysica Acta, 1955. **17**(4): p. 603-604.

9. Weiner, S., et al., *Rotated plywood structure of primary lamellar bone in the rat: Orientations of the collagen fibril arrays.* Bone, 1997. **20**(6): p. 509-514.

10. Kikuchi, M., et al., *Biomimetic synthesis of bone-like nanocomposites using the self-organization mechanism of hydroxyapatite and collagen.* Composites Science and Technology, 2004. **64**(6): p. 819-825.

11. Zhang, L.J., et al., *Hydroxyapatite/collagen composite materials formation in simulated body fluid environment.* Materials Letters, 2004. **58**(5): p. 719-722.

12. Rabinovych, O., et al., *NANOJET as a chemical scalpel for accessing the internal 3D-structure of biological cells.* Microelectronic Engineering, 2004. **73-74**: p. 843-846.

13. Rangelow, I.W., J. Voigt, and K. Edinger, *"NANOJET": Tool for the nanofabrication.* Journal of Vacuum Science & Technology B, 2001. **19**(6): p. 2723-2726.

14. Gutsmann, T., et al., *Evidence that collagen fibrils in tendons are inhomogeneously structured in a tubelike manner.* Biophysical Journal, 2003. **84**(4): p. 2593-2598.

15. Venturoni, M., et al., *Investigations into the polymorphism of rat tail tendon fibrils using atomic force microscopy.* Biochemical and Biophysical Research Communications, 2003. **303**(2): p. 508-513.

16. Raspanti, M., et al., *Direct visualization of collagen-bound proteoglycans by tapping-mode atomic force microscopy.* Journal of Structural Biology, 1997. **119**(2): p. 118-122.

17. Hassenkam, T., et al., *High-resolution AFM imaging of intact and fractured trabecular bone.* Bone, 2004. **35**(1): p. 4-10.

18. Katz, E.P., et al., *The Structure of Mineralized Collagen Fibrils.* Connective Tissue Research, 1989. **21**(1-4): p. 479-488.

19. Currey, J.D., *Mechanical Consequences of Variation in Mineral Content of Bone.* Journal of Biomechanics, 1969. **2**(1): p. 1&.

20. Rho, J.Y., et al., *Variations in the individual thick lamellar properties within osteons by nanoindentation.* Bone, 1999. **25**(3): p. 295-300.

21. Burr, D.B., et al., *Does microdamage accumulation affect the mechanical properties of bone?* Journal of Biomechanics, 1998. **31**(4): p. 337-345.

22. Reilly, G.C. and J.D. Currey, *The effects of damage and microcracking on the impact strength of bone.* Journal of Biomechanics, 2000. **33**(3): p. 337-343.

23. Zioupos, P., et al., *Experimentally Determined Microcracking around a Circular Hole in a Flat-Plate of Bone - Comparison with Predicted Stresses.* Philosophical Transactions of the Royal Society of London Series B-Biological Sciences, 1995. **347**(1322): p. 383-396.

24. Zioupos, P., *Accumulation of in-vivo fatigue microdamage and its relation to biomechanical properties in ageing human cortical bone.* Journal of Microscopy-Oxford, 2001. **201**: p. 270-278.

25. Schaffler, M.B., K. Choi, and C. Milgrom, *Aging and matrix microdamage accumulation in human compact bone.* Bone, 1995. **17**(6): p. 521-525.

26. Nalla, R.K., J.H. Kinney, and R.O. Ritchie, *Mechanistic fracture criteria for the failure of human cortical bone.* Nature Materials, 2003. **2**(3): p. 164-8.

27. Yeni, Y.N. and D.P. Fyhrie, *Collagen-Bridged microcrack model for cortical bone tensile strength.* ASME Bioengineering conference, 2001. **50**: p. 293-294.

28. Weiner, S. and H.D. Wagner, *The material bone: Structure mechanical function relations.* Annual Review of Materials Science, 1998. **28**: p. 271-298.

29. Weiner, S., W. Traub, and H.D. Wagner, *Lamellar bone: Structure-function relations.* Journal of Structural Biology, 1999. **126**(3): p. 241-255.

30. Augat, P., et al., *Anisotropy of the elastic modulus of trabecular bone specimens from different anatomical locations.* Medical Engineering & Physics, 1998. **20**(2): p. 124-131.

31. Hasegawa, K., C.H. Turner, and D.B. Burr, *Contribution of Collagen and Mineral to the Elastic-Anisotropy of Bone.* Calcified Tissue International, 1994. **55**(5): p. 381-386.

32. Goldstein, S.A., et al., *Measurement and Significance of 3-Dimensional Architecture to the Mechanical Integrity of Trabecular Bone.* Calcified Tissue International, 1993. **53**: p. S127-S133.

33. Turner, C.H., A. Chandran, and R.M.V. Pidaparti, *The Anisotropy of Osteonal Bone and Its Ultrastructural Implications.* Bone, 1995. **17**(1): p. 85-89.

34. Bidanset, D.J., et al., *Binding of the proteoglycan decorin to collagen type VI.* J Biol Chem, 1992. **267**(8): p. 5250-6.

35. Fisher, L.W., et al., *Proteoglycans of developing bone.* J Biol Chem, 1983. **258**(10): p. 6588-94.

36. Franzen, A. and D. Heinegard, *Characterization of Proteoglycans from the Calcified Matrix of Bovine Bone.* Biochemical Journal, 1984. **224**(1): p. 59-66.

37. Rees, S.G., et al., *Interaction of bone proteoglycans and proteoglycan components with hydroxyapatite.* Biochimica Et Biophysica Acta-General Subjects, 2001. **1568**(2): p. 118-128.

38. Sodek, K.L., et al., *Relationships between bone protein and mineral in developing porcine long bone and calvaria.* Bone, 2000. **26**(2): p. 189-198.

39. Thompson, J.B., et al., *Bone indentation recovery time correlates with bond reforming time.* Nature, 2001. **414**(6865): p. 773-776.

40. Smith, B.L., et al., *Molecular mechanistic origin of the toughness of natural adhesives, fibres and composites.* Nature, 1999. **399**(6738): p. 761-763.

41. Young, M.F., et al., *Biglycan knockout mice: New models for musculoskeletal diseases.* Glycoconjugate Journal, 2003. **19**(4-5): p. 257-262.

Figure captions:

Figure 1: High resolution images of the primary components of bone. A) AFM image of the outer surface of human trabecular bone. The outer surface consists mainly of collagen fibrils showing the characteristic 67nm D-banding. B) AFM image of mineralized fibrils on a fracture surface of bovine trabecular bone. Here, in the interior of a trabecula, the collagen fibrils are mineralized with hydroxyapatite particles to form the primary building block of bone.

Figure 2: The amount of non-fibrillar and unmineralized organic matrix in trabecular bone varies. The images are taken within 2×2 mm on the same bone sample. A) Fibrils coated with a large amount of non-fibrillar organic material. Particles can still be seen through the smooth cover layer. B) Unmineralized collagen fibrils showing the characteristic 67nm banding pattern. Some particles are between the fibrils but the fibrils are not fully mineralized. C) Mineralized fibrils without non-fibrillar matrix. D) Crack formation in an area with large amounts of non-fibrillar organic matrix. The non-fibrillar organic matrix spans the crack and appears to resist the separation of the mineralized fibrils.

Figure 3: Treatment of bone fracture surface with Nanojet. A) Schematic of Nanojet principle; thermal reactive radicals are released from a 300 nm nozzle that can be scanned with respect to the sample. B) Fracture surface after one hour treatment with Nanojet. The organic surface layer has been removed and the mineral crystals become visible. C) Same sample area after etching two hours.

Further degeneration of the organic matrix forms a rougher surface topography. D) After three hours of etching, the fibrous composition of the bone is visible. The minerals stay in the fibrous form although much of the organic matrix is removed.

Figure 4: Types of filaments that span microcracks in fractured bovine trabecular bone. A) End of a delamination crack. B) Within the crack, filaments span the extent of the crack. The fracture surface appears fibrous. C) Microcracks in a piece of fractured bone. The cracks originate from delamination and parallel translation of the bone. D) Enlargement of the fibrils that span the microcrack. The filaments appear coated and originate from previously parallel positioned fibrils. E) SEM Image of the three main filament types that span the cracks: 1) mineralized fibril bundles that consist of the same material as the bulk of the bone; 2) unstructured, stringy cross-links; 3) bare collagen fibril, the fibril shows the typical 67 nm banding pattern of collagen type I fibrils. The fibril is embedded at the end in the unstructured substance that forms the cross-links described in number 2. F) Magnified view of the bare collagen filament. The fibril shows the typical 67 nm banding pattern (large white arrows) and the recently described small banding (small gray arrows) [15].

Figure 5: Fibrils span cracks in bovine trabecular bone and break after the strain is increased. A) Environmental SEM image of a crack in bovine trabecular bone at 3°C and ≈100% humidity. Several fibrils span the crack. B) Higher

magnification view of a bundle of fibrils that span the gap. C) After the strain on the bone was increased, the crack opened and the fibril was broken.

Figure 6: Overview images of human trabecular bone. The bone consists of a bi-continuous network of trabeculae and voids (normally filled with marrow *in vivo*). Parts A and B show different magnifications.

Figure 7: SEM images of fractured bovine trabecular bone. A) Fracture surface reveals fibrous structure in the bone, following the shape of the outside trabecular surface. B) Fracture occurs by separation of bundles of coated fibrils. C) Filaments are linked to each other in several places by cross connections. The bridges have the same appearance as the fibrils of the bundles. D) The cross-links are on both sides embedded in the main fibrils. These bridges could be preexisting cross-links or could be fibrils that were previously parallel to the others and are now part of two bundles.

Figures:

Figure 1:

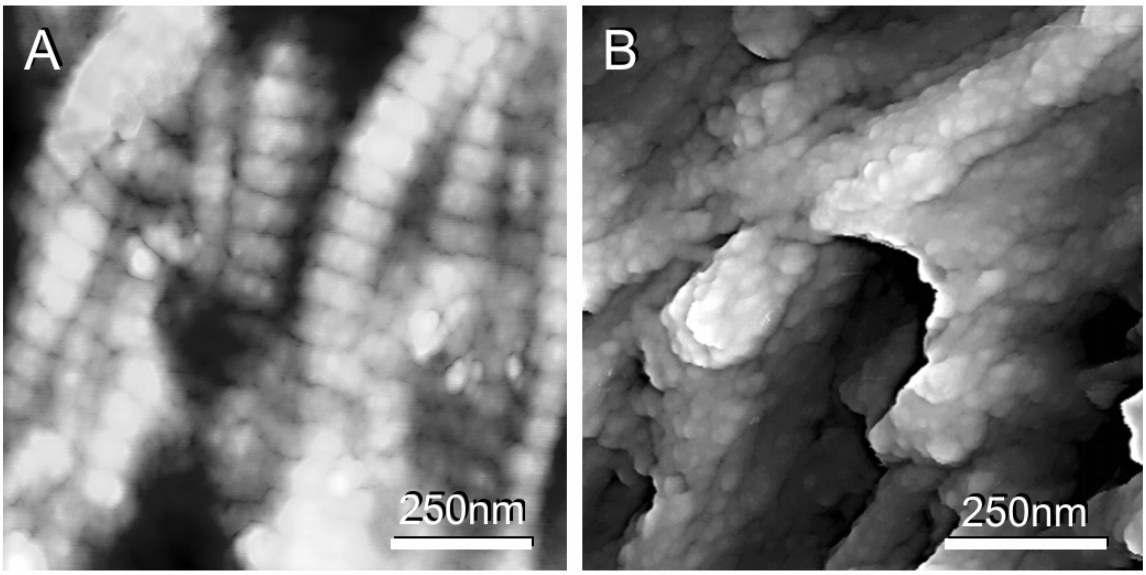

Figure 2:

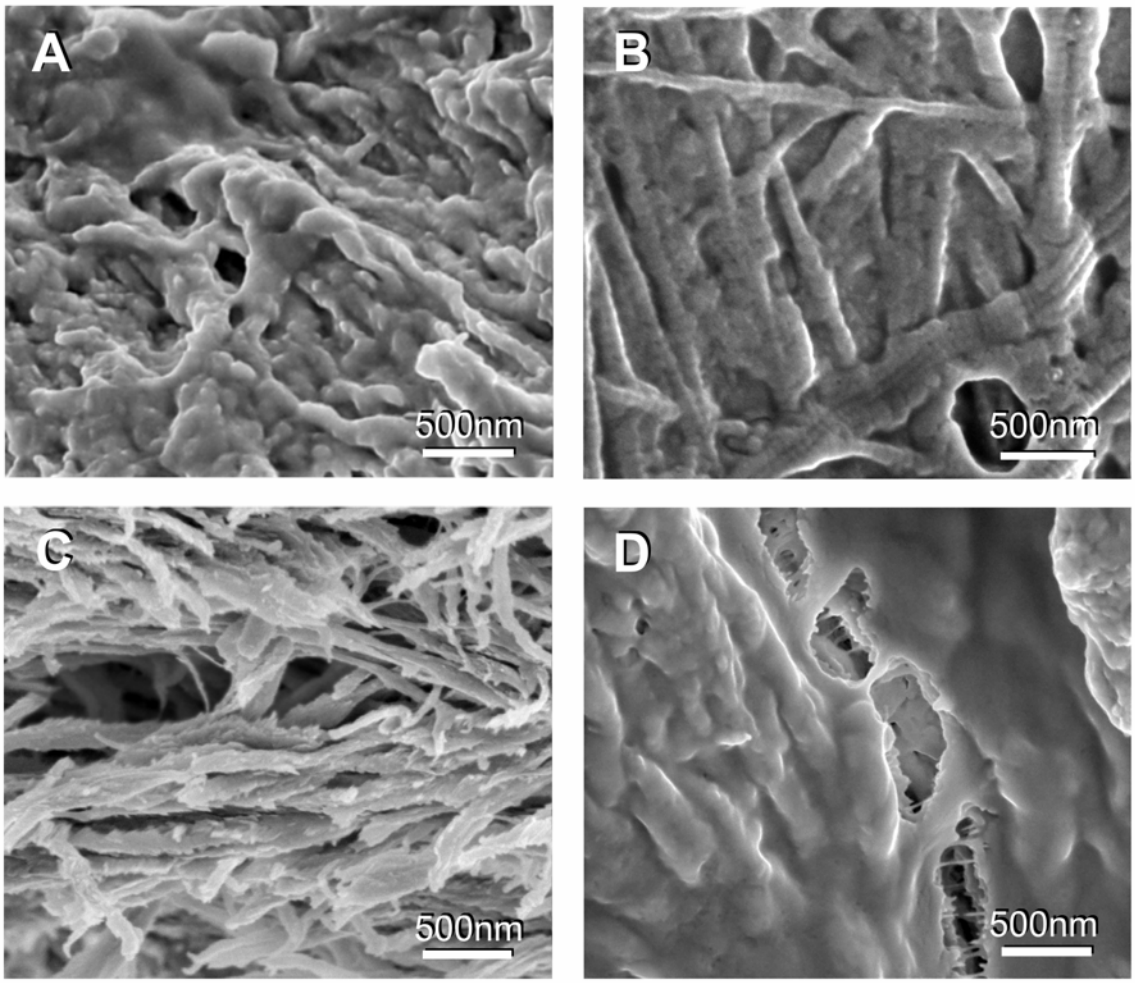

Figure 3:

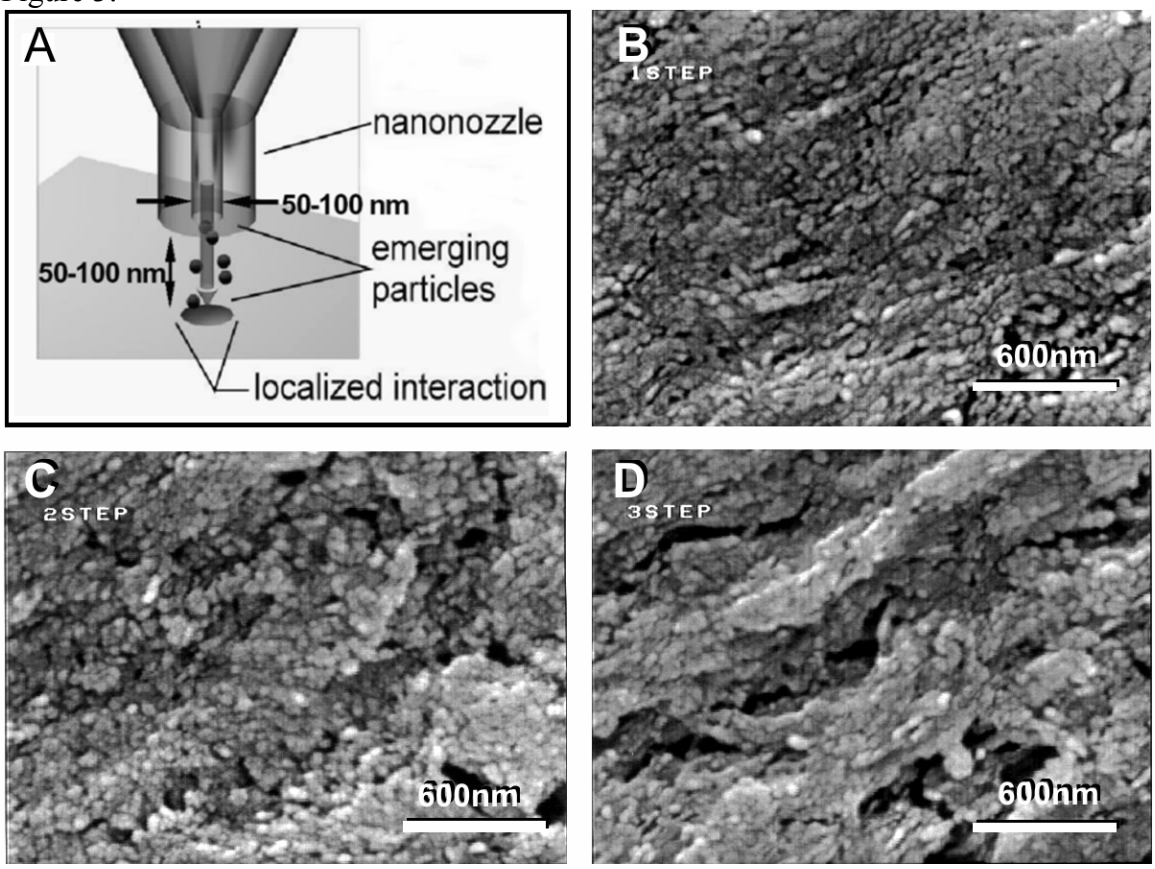
A
nanonozzle
50-100 nm
50-100 nm
emerging
particles
localized interaction
B
1STEP
600nm
C
2STEP
600nm
D
3STEP
600nm

Figure 4:

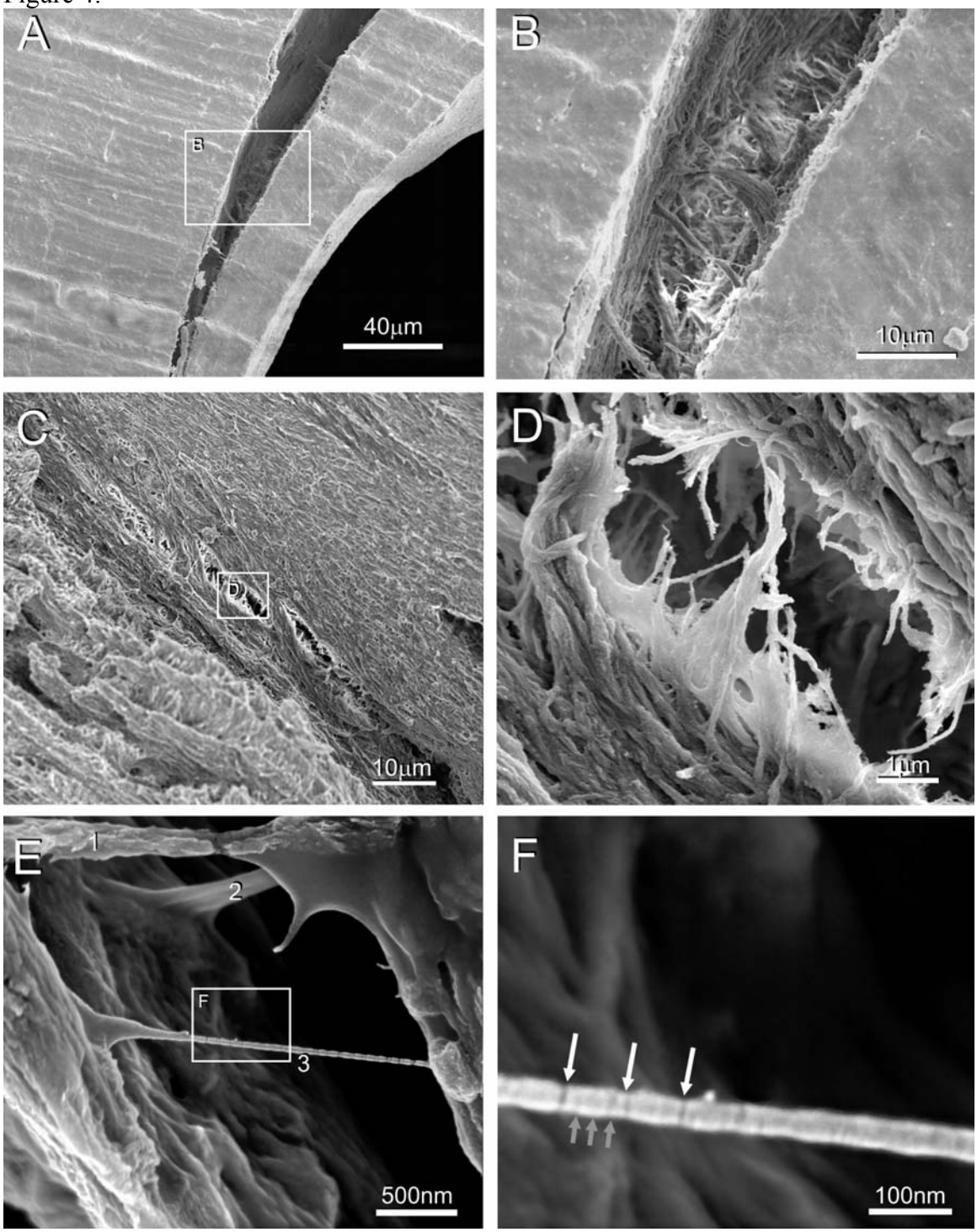

Figure 5:

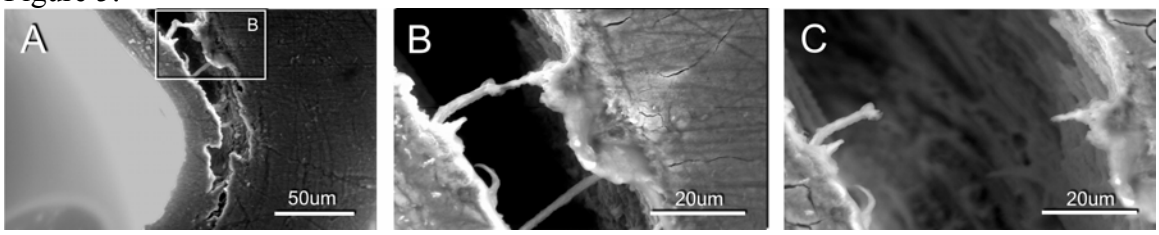

Figure 6:

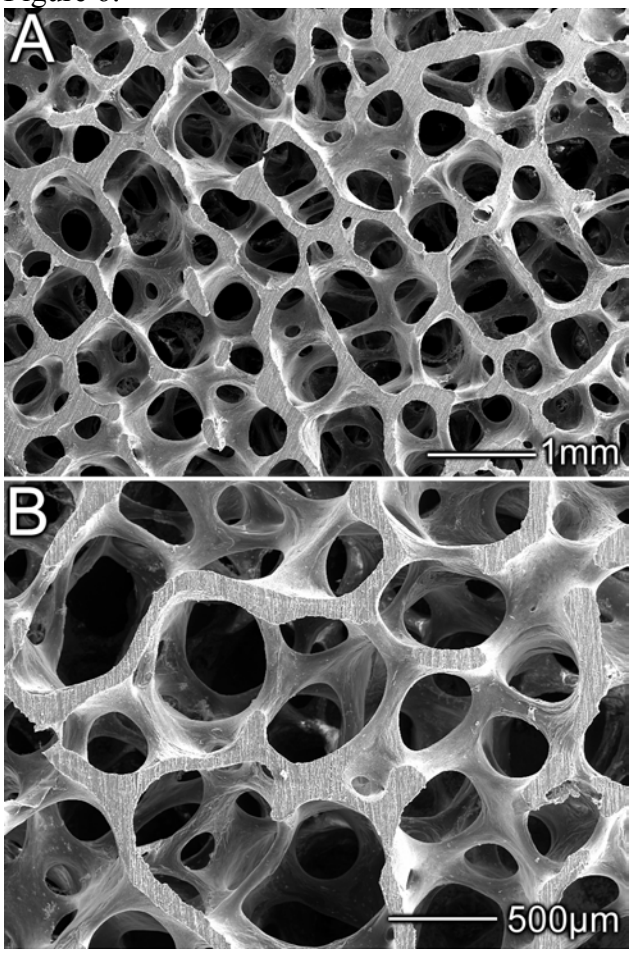

Figure 7: